Lawrence Berkeley Laboratory
UNIVERSITY OF CALIFORNIA

Materials & Molecular Research Division

Submitted to Applied Optics

OPTICAL EFFICIENCY OF FAR-INFRARED PHOTOCONDUCTORS

J.-Q. Wang, P.L. Richards, J.W. Beeman,
N.M. Haegel, and E.E. Haller

July 1986

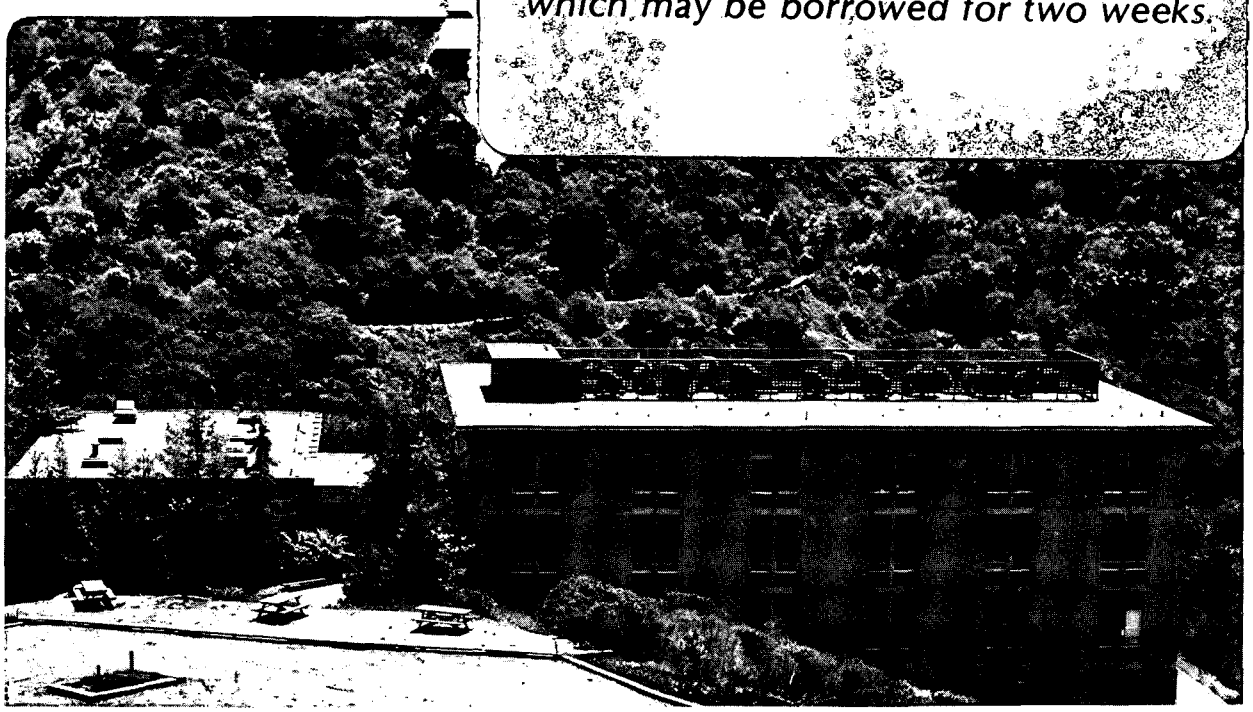

Prepared for the U.S. Department of Energy under Contract DE-AC03-76SF00098

DISCLAIMER

LBL-21958

To be submitted to Applied Optics

OPTICAL EFFICIENCY OF FAR-INFRARED PHOTOCONDUCTORS

J-Q. Wang and P. L. Richards

University of California, Department of Physics
and Lawrence Berkeley Laboratory
Materials and Molecular Research Division
Berkeley, California 94720

and

J. W. Beeman, N. M. Haegel, and E. E. Haller

University of California, Department of Materials Sciences
and Lawrence Berkeley Laboratory
Engineering Division
Berkeley, California 94720

Abstract

We report an experimental and theoretical study to optimize the geometry of far-infrared photoconductive detectors with diffraction limited throughput. Factors considered in this optimization include internal optical path relative to measured absorption length, photoconductive gain, uniformity of illumination, cosmic ray cross section, and compatibility of the design with the requirements of one- and two-dimensional arrays. A rod-shaped detector geometry with square cross section, electrodes on the lateral faces, and a beveled backface to trap the radiation by total internal reflection, was found to have nearly equal responsivity to the best detectors in integrating cavities.

Key words: far infrared photoconductivity, detector efficiency.

I. Introduction

Photoconductive detectors made from germanium doped with acceptors such as gallium and beryllium are used when sensitive far-infrared measurements are made over the wavelength range from 30 to 240 μm. The most stringent requirements on detector sensitivity are encountered in connection with space astronomy experiments which employ cooled optics. Projects such as the proposed NASA Space Infrared Telescope Facility (SIRTF) require both one- and two-dimensional arrays of carefully optimized extrinsic Ge photoconductors with diffraction limited throughput.

An overall optimization of all parameters of such photoconductive detectors is a very complicated task. The detector size, shape, materials parameters, operating temperature and bias must be selected to optimize the required combination of responsivity, detective quantum efficiency, dark current and cosmic ray cross section. In this paper we restrict our attention to an optimization of the size and shape of these detectors.

To proceed with this more limited goal, we must identify the ways in which the important figures of merit depend on detector dimensions. We will show that the optimization of detector size and shape can be carried out independently of other material and operating parameters once the required throughput and the absorption length for infrared in the material are known.

In order to minimize limitations due to amplifier noise at very low illumination it is necessary to maximize the responsivity, which is the ratio of photocurrent I to incident photon rate $\dot{N}$. The responsivity can be written as a product of the electronic charge e, the photoconductive gain g, and the responsive quantum efficiency η_R

$$I/\dot{N} = eg\eta_R \tag{1}$$

The photoconductive gain is defined as the ratio of the carrier lifetime to the transit time between the electrodes which are separated by the distance d. The dependence of g on detector dimensions arises from the transit time. If parameters such as the doping, temperature and bias field are kept fixed, the simplest (uniform field) models of detector operation predict that gain varies as d^{-1}. More realistic models, which predict a non-uniform field distribution in the direction of current flow,[1] also suggest that g will increase with decreasing d.

The responsive quantum efficiency $\eta_R = \varepsilon_o\varepsilon_c$ can be written as the product of the optical efficiency ε_o with which incident photons are absorbed and the efficiency ε_c with which absorbed photons liberate mobile carriers. The optical absorption efficiency ε_o depends on detector dimensions in a straightforward way. It can be made large by minimizing reflection loss at the entrance to the detector and by selecting detector dimensions such that the optical path inside the detector is longer than the absorption length. The efficiency of generation of free carriers

depends only on material parameters such as the cross section for the generation of free carriers compared with the total cross section which also includes contributions from the excitation of electrons into bound states and from the generation of phonons. These parameters influence the selection of the best acceptor density and thus help to determine the absorption length, but do not otherwise affect our optimization.

In many detector applications, amplifier noise can be reduced below photon noise and intrinsic detector noise, so the detective quantum efficiency η_D becomes an important figure of merit. The noise equivalent photon rate in a photoconductive detector can be written in terms of this parameter,

$$\dot{NEN} = (4\dot{N}/\eta_D)^{1/2} . \qquad (2)$$

The detective quantum efficiency η_D is equal to the responsive quantum efficiency η_R if there are no noise mechanisms in addition to photo-generation of carriers and the resulting recombination. If there are additional noise mechanisms, $\eta_D < \eta_R$. We have already discussed how η_R enters our optimization. Detector dimensions must be selected to minimize excess noise mechanisms. Mechanisms to be considered include possible contributions to the dark current due to surface currents, and noise phenomena which arise from nonuniform illumination [2] or nonuniform electric field distributions transverse to the direction of current flow.[2]

In space experiments, cosmic rays can interfere significantly with the desired performance of photoconductive detectors. High

energy photons and charged particles create electron-hole pairs in detector material which cause both noise and an enhancement in detector responsivity.[3-5] Detector size should be minimized to avoid these effects.

Several other factors also favor small detector size. Decreasing the interelectrode distance increases the photoconductive gain. Uniform illumination is more easily achieved in small detectors. However, detector size can only be reduced subject to the need to accept and absorb the incident photons. Also, there can be practical limitations to the smallest detectors that can be fabricated.

The acceptance area of the detector is determined by the required throughput and the focal ratio of the feed optics. For projects such as the Multichannel Imaging Photometer for SIRTF, the angular diameter of the pixels is $\sim\lambda/D$ ($\lambda/2D$ when the focal plane must be fully sampled to obtain super resolution). For a focal ratio of f/3, for example, pixels for λ = 100 μm have diameters of 300 μm (or 150 μm). Focal ratios should be chosen large to minimize detector dimensions, subject to the constraints set by optical aberrations and the ability to fabricate small detectors.

In addition to the pixel diameter, optimum detector geometry depends on the absorption length for infrared in the detector material. The dominant absorption mechanism is proportional to the product of the absorption cross section and the density of the majority impurities. The majority impurity density should be large, subject to the constraint that dark current must be avoided. In Ge:Ga, for example, an acceptor concentration of

$N_A \approx 2\times10^{14}$ cm^{-3} is safely below the threshold for significant dark current due to hopping conduction.[6,7] The possibility of other dark current mechanisms and their dependence on N_A has not been adequately explored. As we will show, this acceptor concentration yields an absorption length of ~5 mm at 100 cm^{-1}, which is the peak of the photoconductive response of Ge:Ga in zero stress. Optical paths of this order in the detector are required to obtain efficient absorption. The optimum absorption length is not well known for Ge:Be or stressed Ge:Ga detectors, but could be significantly different.

The responsivity of a photoconductive detector depends on the bias voltage. The optimum bias voltage is in turn sensitive to the acceptor concentration N_A, the compensation ratio K,[1,6,7] and the amount of breakdown noise that can be tolerated.[1] This complicated behavior does not influence the optimization of the size and shape of detectors made from a given material, except through nonlinearities in the dependence of photoconductive gain and breakdown voltage on the interelectrode distance.[1] In principle, the trade-off between optical efficiency and photoconductive gain could lead to different optimum interelectrode distances for low background applications where amplifier noise is important, and high background applications where amplifier noise is not important. In practice, these dependences are weak; so our optimization experiments are carried out for a single interelectrode distance to avoid confusion in

selecting comparable bias field conditions for detectors with different separations.

We conclude from this analysis that if we are given the required pixel diameter and the optimum absorption length, we can find an optimum shape and size for far-infrared photoconductive detectors without reference to other material or operating parameters. In this paper we explore this optimization for 0.5×0.5 mm^2 pixels and an absorption length of 5 mm. Our results can be scaled to other values of these parameters. To avoid chaotic phenomena,[1-2] we choose to consider only geometries for which the photocurrent is uniformly distributed. That is, we require that the detector material be nearly uniformly illuminated and that the detector cross section parallel to the electrodes be constant.

Detectors made from materials such as extrinsic Si, for which the absorption length is comparable to or less than the pixel diameter, often make use of infrared illumination through a transparent front electrode. Despite major advantages for the fabrication of arrays, this geometry does not appear competitive for materials with long absorption lengths, because of the large sacrifice in photoconductive gain.

We have compared two generic detector geometries. One is a flat rectangular detector in a metallic cavity with electrodes on the broad faces, such as the one shown in Fig. 1 a). The other is a rod-shaped detector with square cross section which has electrodes on two of the lateral faces, such as is shown in Fig. 1 b). This detector is illuminated on one end; the other end is

beveled so as to trap the radiation by total internal reflection. We use the term "end-fire" to describe this detector. Both detector designs are well known to the far-infrared detector community, but there is no consensus as to which is preferable. We have not been able to identify the origins of either of these designs.

II. Measurements of Absorption Length

The absorption length, or its reciprocal the frequency dependent absorption coefficient $\alpha(\nu)$, is an important parameter for detector material. We have used measurements of far-infrared transmittance to determine the absorption coefficients in Ge:Ga with a large (100) stress, unstressed Ge:Ga, and Ge:Be detector materials. In the stressed sample the direction of propagation of unpolarized radiation was perpendicular to the axis of the stress. Since the dominant contribution to $\alpha(\nu)$ in the frequency range of interest is proportional to the acceptor concentration N_A, it is different in different detector materials. In Table I we list the values of N_A and compensation ratio K for our samples as determined from Hall effect measurements as a function of temperature.

Our measurements of $\alpha(\nu)$ can be easily scaled to any available detector or detector material by measuring the room temperature conductivity to determine N_A. For Ge:Ga we have the relation $N_A(cm^{-3}) = 2.8\times10^{15}\ \sigma_{300}(\text{ohm cm})^{-1}$. The origin of this convenient relation can be understood by expressing the conductivity as the product of the hole mobility μ, the electronic charge e, and the hole density p, $\sigma=\mu ep$. The mobility of free

carriers in Ge is limited by phonons at 300 K in the useful range of concentration, so is independent of N_A. Since the impurity states are ionized at 300 K, but excitation across the band gap can be neglected, $p=N_A$. Thus we have $N_A = \sigma/\mu e$. The same argument can be used for Ge:Be, except that the double acceptor Be yields two mobile holes at 300 K. As a result,

$N_A = 1.4\times10^{+15}\ \sigma_{300}$ for Ge:Be.

Infrared absorption coefficients were determined from measurements of normalized sample transmittance made at 1.2 K with a Fourier transform spectrometer and bolometric detector. An example of the transmittance of Ge:Ga (with uniaxial stress) is shown in Fig. 2. Interference fringes which arise from parallel sample faces are clearly visible. The transmittance scale contains uncertainties due to the partial saturation of the bolometer when the sample was removed to obtain a reference spectrum. Changes in the optical path when a high-index medium was inserted or removed caused additional uncertainties. The most precise value of the scale factor was obtained as follows: The index of refraction $n = (2\delta\nu d)^{-1}$ was measured from the fringe separation $\delta\nu$ and sample thickness d. The measured value n=4.0 is very close to the zero frequency value for pure Ge and is independent of frequency, impurity content and stress. The dielectric reflectance $R = [(n-1)/(n+1)]^2 = 0.36$ was then computed. The experimental value of the transmittance averaged over the interference fringes at low frequencies, where absorption can be neglected, was then adjusted to equal the theoretical value $T = (1-R)/(1+R) = 0.47$.

The frequency-dependent absorption coefficient $\alpha(\nu)$ was computed from the measured $T(\nu)$, averaged over interference fringes, and the computed R from the equation

$$\exp[-\alpha(\nu)d] = \frac{1}{2TR^2}\{[(1-R)^4 + 4R^2T^2]^{1/2} - (1-R)^2\} \qquad (3)$$

This equation can be derived by adding the intensities of multiple reflections, or alternatively by averaging the full expression[8] over interference fringes in the limit $k/n << 1$. In this limit, R is independent of frequency, even in the lossy region above threshold.

The measurements of $\alpha(\nu)$ shown in Fig. 3 were deduced from transmittance measurements on the samples listed in Table I. Relatively thin d = 1.4 mm samples were used to clearly show the interference fringes as in Fig. 2. Thicker samples were also used to emphasize the absorption. In each plot, $\alpha(\nu)/N_A$ is given as a dashed line over the frequency range in which the absorption is dominated by transitions between bound states which do not cause a photocurrent, and by a solid line above the threshold for photoconductivity where the cross section is dominated by transitions from the acceptor ground state to the band.

The transition region between these two limits is quite complicated and depends on N_A through the broadening of bound state levels by interactions between acceptor centers. Measured values of α/N_A in unstressed Ge:Ga for $N_A = 1.2\times10^{14}$ and 1.8×10^{14} cm^{-3} are the same above 110 cm^{-1}, but vary by 15% at 90 cm^{-1}. The peak in the photoresponse occurs at 100 cm^{-1}. The useful frequency range for Ge:Be detectors extends above 300 cm^{-1} where phonon absorption (that is not proportional to N_A) becomes important.[9]

The large change in $\alpha(\nu)$ with stress deserve some comment. A uniaxial stress applied along the (100) axis of Ge lifts the degeneracy at the center of the valence band and reduces the binding energy of shallow acceptors such as Ga by a factor[10,11] approaching 2. The utility of the stressed Ge detector arises from the resulting shift of the photoresponse to lower frequencies. The shallow acceptor state for the non-degenerate band is analogous to the hydrogen atom and the cross section falls rapidly with frequency above the threshold.[12] The cross section of the acceptor state for the degenerate band of unstressed Ge:Ga evidently varies more slowly with frequency.

The increase in α with stress arises from an increase in the absorption cross section which can be estimated from an increase in the area of the effective Bohr orbits. In zero stress the average value of $|r|$ weighted by the probability density in the ground state[13] is a = 75 Å. In a large (100) stress the wave function spreads and elongates in the direction of the stress[14] so that $a_{\parallel}$ = 129 Å and $a_{\perp}$ = 93 Å. This picture leads us to expect an increase in α by a factor ~2 for light propagating perpendicular to the stress axis, which is comparable to the observed effect.

Our measurements give the relationship between α and N_A. They do not tell us the optimum extinction length, unless the optimum value of N_A is known. Unstressed Ge:Ga detectors typically have $N_A \simeq 2\times10^{14}$ cm^{-3}. Since the hopping contribution to the dark current depends on the wavefunction overlap in the direction of current flow, we can anticipate that the optimum N_A will be

somewhat smaller for stressed Ge:Ga detectors. We have used Ge:Ga with $N_A = 1.2 \times 10^{14}$ cm^{-3} for stressed detectors, but the dark current has not yet been measured. Successful Ge:Be detectors with very low dark current[15] have been made using Be concentrations greater than 7.5×10^{14} cm^{-3}.

III. Design of Test Detectors

In order to determine the detector design with the best optical efficiency, it is necessary to compare optimized versions of each competing detector type. Since diffraction effects limit the validity of theoretical calculations, we must rely on a limited number of experimental comparisons. Comparisons between the responsivities of different detectors are meaningful indicators of optical efficiency only if the detectors are made from the same materials, have the same interelectrode distance and the same kind of kind of contacts, and are operated at the same temperature and bias. In order to achieve these conditions, we use detectors with a single interelectrode separation d = 0.5 mm, which were cut from a single wafer of Ge:Ga whose acceptor concentration is very homogeneous, as determined from measurements of the room temperature conductivity. The entire wafer was implanted with B^+-ions, metallized and annealed as described in Ref. 6 to insure contact uniformity. A portion of the wafer was left unmetallized to make a detector with transparent electrodes.

Two generic detector geometries are commonly used when the extinction length is an order of magnitude longer than the required pixel diameter. In one approach the detector is located in a metallic integrating cavity whose entrance aperture is

determined by the required pixel diameter. The idea is that photons which are not absorbed by the detector on the first pass are given further opportunities after reflection from the cavity walls. The use of a cavity is thought to provide good absorption efficiency in a smaller detector with more uniform illumination. The performance of such cavities can be analyzed quantitatively in the geometrical optics approximation by computer ray tracing or by a statistical approach[16] which assumed a random distribution of photons in the cavity. Accurate predictions are not possible with either approach for diffraction limited pixel diameters, however, because diffraction effects are important. In practice, many favorite cavity designs exist and there is little evidence to support preferences between them.

Figure 1 a) shows a 0.5×2×2 mm detector with electrodes on the large faces located in a brass cavity which has axial symmetry about the detector post. The cavity is designed to avoid parallel faces and to keep the area of the metal walls small. Experiments showed that the best response was obtained with the vertical position of the detector adjusted to be in line with the entrance aperture and the detector rotated so that reflections from its front face could not escape directly out of the aperture. A smaller 0.5×1×1 mm detector was installed in a cavity with similar proportions, but smaller diameter.

The large cavity detector with metallized electrodes suffers from the fact that only a third of the detector surface area can accept photons. Truly transparent electrodes should improve the optical efficiency or reduce the required detector dimensions.

Semi-transparent electrodes made by B^+-ion implantation without metallization absorb[17] significantly more than cavity walls or metallic electrodes. Measurements were made of the infrared transmittance of a 0.5 mm wafer of sample 2 which was implanted on both sides and annealed according to the prescription in Ref. 6, but not metallized. The measured transmittance was fitted to a theory[18] of the transmittance of a dielectric slab with the known value of n and $\alpha(\nu)$ and with thin conducting films on both sides. The fit gave a sheet conductance for each implanted layer of 360 $\Omega/\square$. The infrared transmittance for a single surface is 43%. The absorptance for a ray passing from vacuum to detector is 11%, and for a ray passing from detector to vacuum is 45%. A large (2×2 mm) cavity detector was made from this material.

The second generic detector is rod shaped with square cross section as is shown in Fig. 1 b). The transverse dimensions are set by the pixel size and the length is chosen to obtain efficient absorption. To keep the interelectrode distance small, the electrodes are located on lateral faces. The loss of photons from the sides of such detectors is small because of total internal reflection from the open Ge sides and the high reflectivity of the metallic electrodes. Losses in internal reflection from an implanted and metallized contact are expected to be much smaller than for the same implanted layer in a transparent contact because the metal boundary creates a null in the parallel infrared E-field close to the location of the implanted layer. For grazing incidence the loss is zero for an E-field perpendicular to a conducting sheet or surface.

The detector length required to absorb efficiently can be reduced by cutting the back face at an angle ≈20° as shown in Fig. 1 b) and Fig. 4. Rays propagating parallel to the optic axis are then totally reflected at the back face. As shown in Fig. 4 a) and b) these rays make a total of either three or four passes along the detector before any radiation can escape. The detailed dependence of the average number of passes on detector length is quite complicated. To a good approximation, however, the average optical path inside the detector with a 20° bevel is 4.1 times the average detector length.

Because the index of refraction n = 4 of Ge is quite large, this analysis remains valid for significant angles of incidence. Infrared incident with a focal ratio f/3 outside the detector, for example, forms an internal cone of rays with half angle only 2.4° about the detector axis. Since the cutoff angle for total internal reflection is 14.5°, all such rays are totally reflected at the 20° back face.

The optical efficiency ε_o of an endfire detector of average length ℓ and absorption coefficient $\alpha(\nu)$ can be estimated from the approximate equation

$$\varepsilon_o = (1-R)\,[1-e^{-\alpha(\nu)L}]/[1-Re^{-\alpha(\nu)L}] \qquad (4)$$

where $L = 4.1\,\ell$. The same equation is exact for a detector with a perpendicular backface, except that $L = \ell$. Again, because of the large index for Ge, the reflection loss R = 0.36 from the detector surface is important. Anti-reflection coatings can be used to reduce this loss without any change in the cutoff angle for total internal reflection at the front face.

When an ideal anti-reflection coating is used on the front surface of the detector, Eq. (4) can be used for end-fire detectors if we set R = 0. When detectors with a perpendicular back face are anti-reflection coated on the front face, the optical efficiency is given by

$$\varepsilon_o = (1 - e^{-\alpha L})\,(1 + Re^{-\alpha L}). \qquad (5)$$

IV. Detector Fabrication

Test detectors were prepared from a 0.5 mm thick slice of sample 2 whose properties are listed in Table I. The wafer was lightly etched, ion-implanted, gold-matallized and annealed on both sides using the prescription in Ref. 6. The interelectrode separation was 0.48 mm. Square samples with nominal dimensions 1×1 mm and 2×2 mm were cut from this wafer for cavity detectors. A 2×2 mm cavity detector was also cut from a section of the wafer that was implanted, but not metallized, so as to give semi-transparent electrodes. Rods 0.5 mm wide were cut from the metallized material. These rods were cut to 0.5 and 1 mm lengths with perpendicular end faces, and both 1 and 2.5 mm average lengths with back faces beveled at 20°.

In order to avoid excessive handling of detectors after etching, the actual detector sizes were determined optically before etching and the size reduction during etching was estimated from witness samples. Values of length, width, and interelectrode separation are listed in Table II. Each detector was mounted on a 0.34 mm diameter gold plated steel rod using Epo-tek H20E conducting epoxy[19] for the metallized detectors, and In solder for the unmetallized detector. An 0.13 mm copper lead was soldered with In to the other detector contact.

V. Experimental detector comparisons

The test apparatus shown in Fig. 5 was designed to provide accurate comparisons of the spectral responsivity of pairs of detectors. The f/1.5 infrared beam from a Fourier transform far infrared spectrometer is chopped at 10 Hz and enters the apparatus through a metal light pipe labeled a, which contains a black polyethylene low-pass filter and a 1% NiCr neutral-density filter at b. These filters were selected to give a photon rate of 5×10^{10} sec^{-1} from 100 to 300 cm^{-1} for an optical throughput of $A\Omega=10^{-4}$ ster-cm^2. The metal roof mirror c divides the beam symmetrically, reflecting it horizontally to left and right. Two sets of apertures labeled d are separated by a cavity coated with Ames 24E [20] optical black. The first aperture, which has a diameter of 1.7 mm and is 7.1 mm in front of the entrance to the detector limits the field of view at the detector to f/4.2 or 0.045 sr. With pixel dimensions of 0.25 mm^2 this gives $A\Omega = \lambda^2$ at λ = 106 μm. The second blackened aperture serves to reduce stray light. In the case of the cavity detectors, the hole in the cavity serves to define the detector acceptance area. It is located immediately behind the second blackened aperture. When endfire detectors were measured, a metal foil with a square hole etched in it was used immediately in front of the detector to define the acceptance area. Endfire detectors measured without this second aperture gave ~35% larger signals because of absorption on the sides of the detector. This absorption is quite efficient because the angles of incidence approach Brewster's angle. Fig. 5 shows an endfire detector e mounted at the right backed by a blackened cavity f used to absorb stray light. This

apparatus was equipped with thermometers and was surrounded with a blackened, light-tight metal can which was immersed in LHe in a glass dewar. The can could either be evacuated or filled with He exchange gas.

This system was used for several different detector comparisons. The spectral responsivity of each of our photoconductive Ge:Ga detectors was compared with that of the detector Cav-2. Detectors were interchanged on several occasions to evaluate the small (~5%) asymmetry of the apertures and repeated measurements were made to test the reproducibility, which was within 5%.

The relative spectral responsivity of the photoconductive detectors was measured by replacing one detector by a composite bolometer with a metal film absorber,[21] as is shown at g in Fig. 5. The far infrared transmittance of the composite bolometer has been measured and shown to be consistent with that expected for a 200 Ω/□ film which has an absorptivity of 50% independent of wavelength.[22] The Ge:Ga photoconductor was operated in a vacuum at 3 K and then the temperature was lowered to 1.2 K for a bolometric measurement with the same spectrometer output. The bolometer signal was used to normalize the spectral response of the photoconductor.

Measurements of the absolute responsivity of photoconductive detectors were made as follows. The responsivity of the bolometer was determined using the standard procedure from the dc load curve and a measurement of the responsivity as a function of chopping frequency.[23] This procedure is not as accurate as one involving a

separate heater on the bolometer,[22] but has been shown to produce results with accuracy ±20% when used with bolometers with ohmic contacts.[22] Once the electrical responsivity of the bolometer and its absorptivity were known, it was used to calibrate the responsivity of the other detectors by using a suitable mask to define the acceptance area of the bolometer.

VI. Summary and Conclusions

The results of our detector comparisons are shown in Table II. The largest responsivity was observed for Cav-1 which was a ~2×2 mm^2 cavity detector with semi-transparent electrodes. The detectors Cav-2 and Cav-3, which were ~2×2 and ~1×1 mm^2 cavity detectors with metallized electrodes, gave progressively smaller responsivities. This is presumably because the absorption in the Ge becomes small compared with the other losses.

Two endfire detectors Ef-1 and Ef-2 with beveled back faces were tested along with two detectors Rect-1 and Cube-1 with perpendicular back faces. All of these detectors suffer a 36% reflection loss. We believe that a suitable anti-reflection coating can recover most of this loss, but have not yet fabricated one. We therefore list both the measured responsivity and (in parentheses) the responsivity corrected to the case of no reflection at the front surface. The ~2.5 mm Ef-1 has essentially the same corrected responsivity as Cav-1. The value of a beveled backface is clearly indicated by a comparison of Ef-2 and Rect-1, both of which are ~1 mm long.

The relative accuracy of these responsivity measurements should be better than ±10%. The absolute accuracy, however, is

lower, perhaps ±30%. The absolute responsivity measurements were obtained with an operating temperature of 3.0 K and a bias voltage of 50 mV where the responsivity was varying as the square of the bias voltage. The breakdown voltage was 170 mV. Although no noise measurements were made, it is believed that this bias is representative of that used in many experiments.

The optical efficiency ε_o of endfire, rectangular and cubic detectors was calculated from Eqs. 4 and 5 using a value of $\alpha = 2.27$ for sample 2 at 100 cm^{-1}. The calculated efficiencies given in Table II show the same qualitative trend as the measured responsivities. The ratio of the measured responsivity to the calculated optical efficiency is a measure of the success of the theoretical model. It is 9.3±0.5 for the endfire detectors and 14±1 for the detectors with perpendicular back faces. This suggests that only two thirds of the predicted benefit of the wedged back face are being realized.

We conclude that the long endfire detector Ef-1 with anti-reflection coating will have a responsivity equal to our best cavity detector. It has significantly smaller cross-section for cosmic rays and is much easier to use with uniaxial stress and to assemble into close-packed one- or two-dimensional detector arrays. Our choice for the optimum detector is thus the anti-reflection coated endfire geometry with length equal to 0.3 to 0.5 times α^{-1}.

Acknowledgments

This work was supported in part by the Director, Office of Energy Research, Office of Basic Energy Sciences, Materials Sciences Division, and in part by NASA Contract No. W-14,606 under Interagency Agreement, Office of Health and Environmental Research of the U.S. Department of Energy under Contract No. DE-AC03-76SF00098.

Table I. Acceptor Concentration and Compensation of Detector Materials

Sample	Material	N_A (cm^{-3})	K
1. LBL 82-head	Ge:Ga	1.2×10^{14}	$\sim10^{-2}$
2. LBL 108-14.6	Ge:Ga	1.8×10^{14}	$\sim10^{-2}$
3. LBL 728-4.9	Ge:Be	7.5×10^{14}	-

Table II. Results of Detector Comparisons

Detector	Dimensions (mm^3)	Pixel Area (mm^2)	Responsivity (A/W)	Optical Efficiency[d] ε_o
Cav-1 [a]	2×2×0.48	0.24	9.3	
Cav-2 [b]	1.94×1.95×0.48	0.24	6.4	
Cav-3 [b]	0.92×0.96×0.49	0.25	4.5	
Ef-1	2.39×0.43×0.48[c]	0.21	5.8 (8.7)[c]	0.59 (0.89)[c]
Ef-2	0.91×0.43×0.48[c]	0.21	3.8 (5.0)	0.43 (0.57)
Rect-1	0.87×0.44×0.48	0.21	2.1 (3.0)	0.16 (0.23)
Cube-1	0.48×0.48×0.48	0.23	1.5 (2.1)	0.10 (0.14)

[a] Semi-transparent electrodes

[b] Metallized electrodes

[c] (Estimated responsivity with an anti-reflection coating on the front surface.)

[d] Calculated from Eqs. 4) and 5).

References

1. R. W. Westervelt and S. W. Teitsworth, "Nonlinear Transient Response of Extrinsic Ge Far-Infrared Photoconductors," J. Appl. Phys. 57, 5457 (1985).

2. S. W. Teitsworth, R. N. Westervelt, and E. E. Haller, "Nonlinear Oscillation and Chaos in Electrical Breakdown in Ge," Phys. Rev. Lett. 51, 825 (1983).

3. H. Aumanm, B. Brown, F. Gillett, W. Irace, D. Langford, P. Mason, and R. Salazar, IRAS In-Orbit Performance Assessment, (Jet Propulsion Laboratory Report 871, 1983), p.19.

4. J. Wolf and D. Lemke, "Tests of Low-Background Infrared Detectors," A.F.M. Moorwood and K. Kjar, Ed., Proc. of the Second ESO Infrared Workshop, (1982), p. 191.

5. N. Oda, D. Lemke, and J. Wolf, "Radiation Effects on a Ge:Ga Photoconductive Detector," Intl. J. Infrared and Millimeter Waves 5, 1499 (1984).

6. E. E. Haller, M. R. Hueschen, and P. L. Richards, "Ge:Ga Photoconductors in Low Infrared Backgrounds," Appl. Phys. Lett. 34, 495 (1979).

7. N. M. Haegel, Performance and Materials Aspects of Ge:Be and Ge:Ga Photoconductors for Far Infrared Detection, MS Thesis, (University of California, Berkeley, 1983), Lawrence Berkeley Laboratory Report 16694.

8. F. Abeles, Ed., Optical Properties of Solids (North-Holland, Amsterdam, 1972), p. 26.

9. R. J. Collins and H. Y. Fan, "Infrared Lattice Absorption Bands in Germanium, Silicon and Diamond," Phys. Rev. 93, 674 (1954).

10. A. G. Kazanskii, P. L. Richards, and E. E. Haller, "Photoionization of Acceptors in Uniaxially Stressed Germanium," Solid State Commun. 24, 603 (1977).

11. A. G. Kazanskii, P. L. Richards, and E. E. Haller, "Far-Infrared Photoconductivity of Uniaxially Stressed Germanium," Appl. Phys. Lett. 31, 496 (1977).

12. H. S. W. Massey, Electronic and Ionic Impact Phenomena (Oxford, 1969), Vol. II, p. 1073.

13. A. Baldereschi and N. O. Lipari, "Spherical Model of Shallow Acceptor States in Semiconductors," Phys. Rev. B 8, 2697 (1973).

14. F. H. Pollak, "Effect of Uniaxial Compression on Impurity Conduction in P-Germanium," Phys. Rev. A138, 618 (1965).

15. N. M. Haegel, E. E. Haller, and P. N. Luke, "Performance and Materials Aspects of Ge:Be Photodetectors," Intl. J. Infrared and Millimeter Waves 4, 945 (1983).

16. W. E. Lamb, Jr., "Theory of a Microwave Spectroscope," Phys. Rev. 70, 308 (1946).

17. V. Hadek, D. M. Watson, C. A. Beichman, and M. D. Jaek, "Far-Infrared Transmittance of Boron-Implanted Germanium at Liquid-Helium Temperatures," Phys. Rev. B 31, 3630 (1985).

18. G. I. Hoffer, Superconducting Junction Bolometers, Ph.D. Thesis (University of California, Berkeley, 1975) Lawrence Berkeley Laboratory Report 3759.

19. Epo-Tek H20E silver epoxy, Epoxy Technology Inc., Billerica, Massachusetts 01821.

20. Black coating AMES-24E obtained from J. M. Smith, NASA Ames Research Center.

21. N. S. Nishioka, P. L. Richards, and D. P. Woody,"Composite Bolometers for Submillimeter Wavelengths," Appl. Optics 17, 1562 (1978).

22. A. E. Lange, E. Kreysa, S. E. McBride, P. L. Richards, and E. E. Haller, "Improved Fabrication Techniques for Infrared Bolometers," Intl. J. Infrared and Millimeter Waves 4, 689 (1983).

23. R. C. Jones, "The General Theory of Bolometer Performance," J. Opt. Soc. Am. 43, 1 (1953).

Figure Captions

Fig. 1. Two generic types of far-infrared detector compared experimentally: a) Cross section of 2×2×0.5 mm detector in a metal cavity. b) Perspective view of 2.5×0.5×0.5 mm endfire detector.

Fig. 2. Far-infrared transmittance at 1.2 K of 1.45 mm of Ge:Ga material 1 with a large uniaxial stress along a (100) axis.

Fig. 3. Ratio of frequency dependent absorption coefficients $\alpha(\nu)$ to acceptor concentration N_A for a) Ge:Ga sample 1 with infrared propagating perpendicular to a large (100) uniaxial stress. b) for Ge:Ga sample 1 with no stress, and c) for Ge:Be sample 3. Typical estimated errors are shown. In the region covered by dashed lines, the absorption is due primarily to transitions to bound states. The solid lines show absorption due primarily to the generation of free carriers. The application of a large stress in the (100) direction increases the peak value of α by a factor 3.

Fig. 4. Two different optical paths through an endfire detector showing a) three and b) four passes before the beam can escape.

Fig. 5. Cross-section of the test apparatus used to compare optical responsivities of far-infrared detectors: a - light pipe, b - filter, c - roof mirror, d - apertures, e - endfire photoconductive detector, f - blackened cone, and g - bolometric detector.

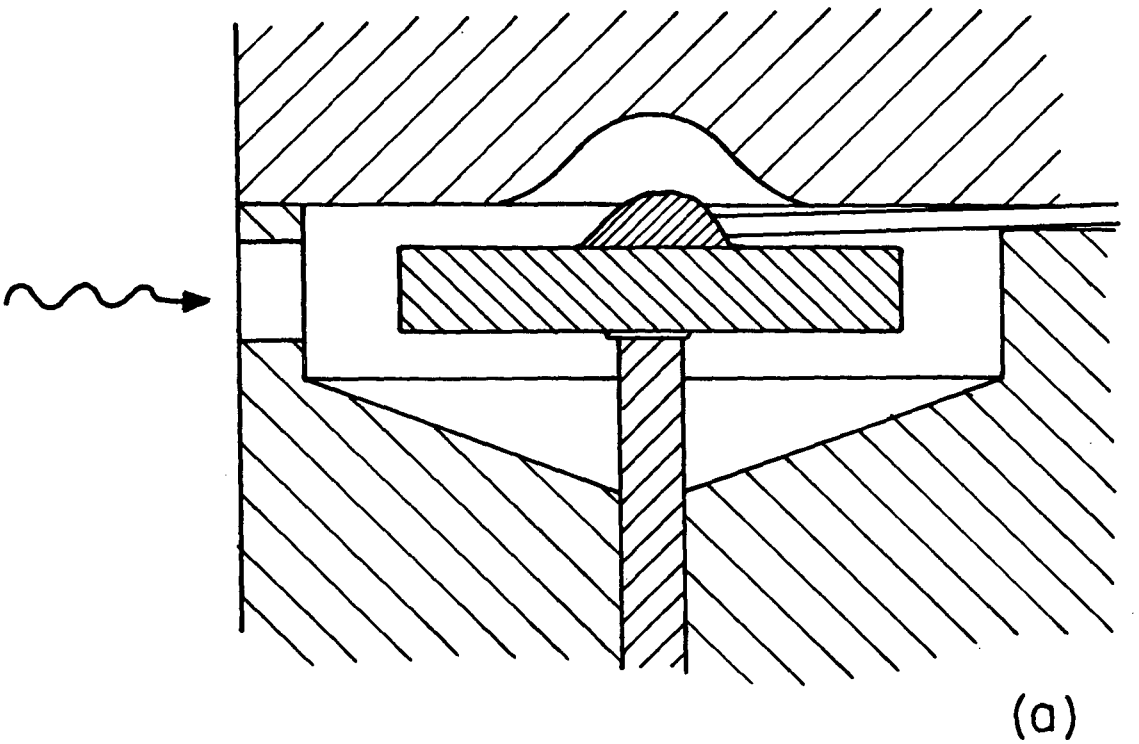

(a)

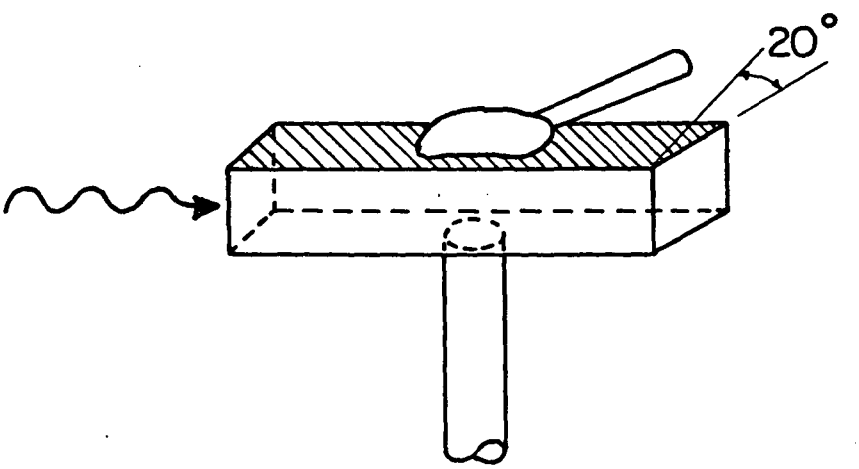

(b)

FIGURE 1

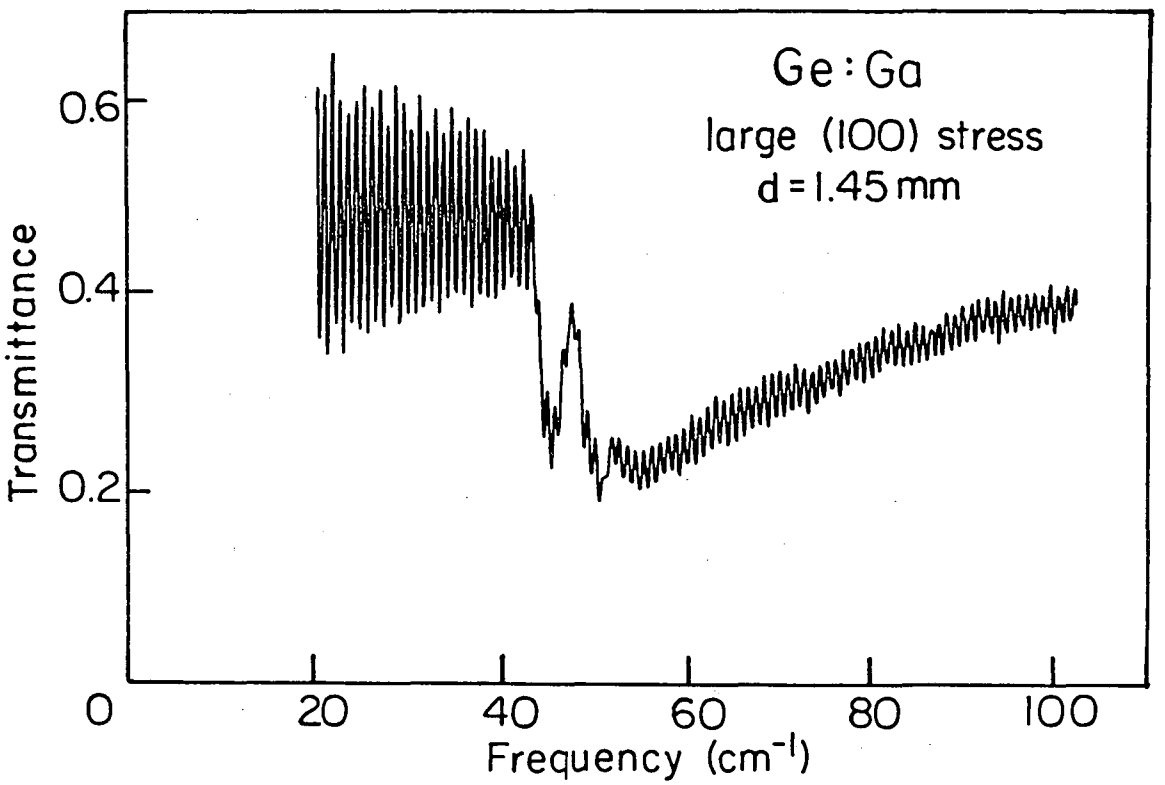
Ge : Ga
large (100) stress
d = 1.45 mm
Transmittance
0.6
0.4
0.2
0
20
40
60
80
100
Frequency (cm⁻¹)

FIGURE 2

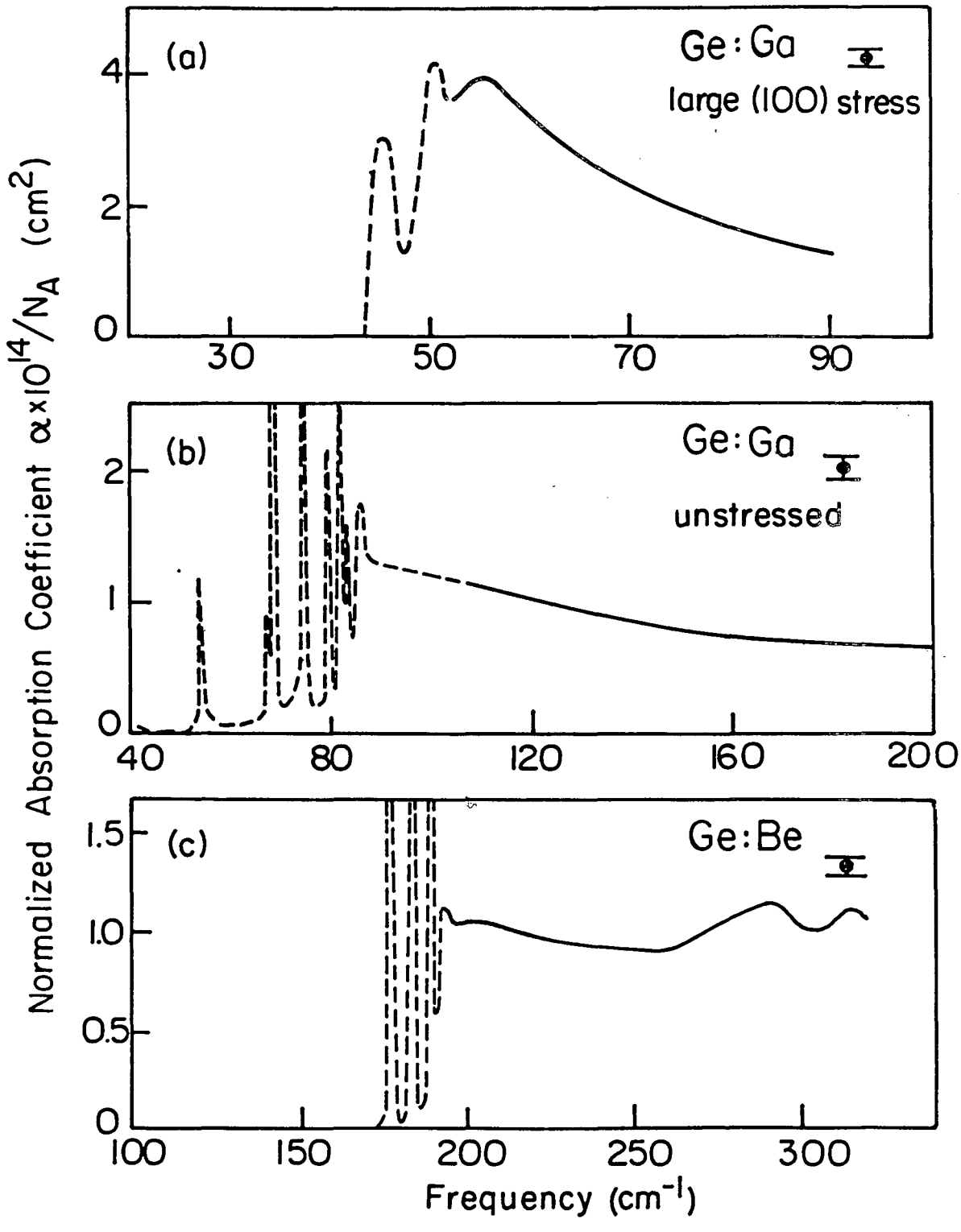
(a)
Ge:Ga
large (100) stress
(b)
Ge:Ga
unstressed
(c)
Ge:Be
Normalized Absorption Coefficient $\alpha \times 10^{14}/N_A$ (cm^2)
Frequency (cm^{-1})
0
2
4
30
50
70
90
1
40
80
120
160
200
0.5
1.0
1.5
100
150
200
250
300

FIGURE 3

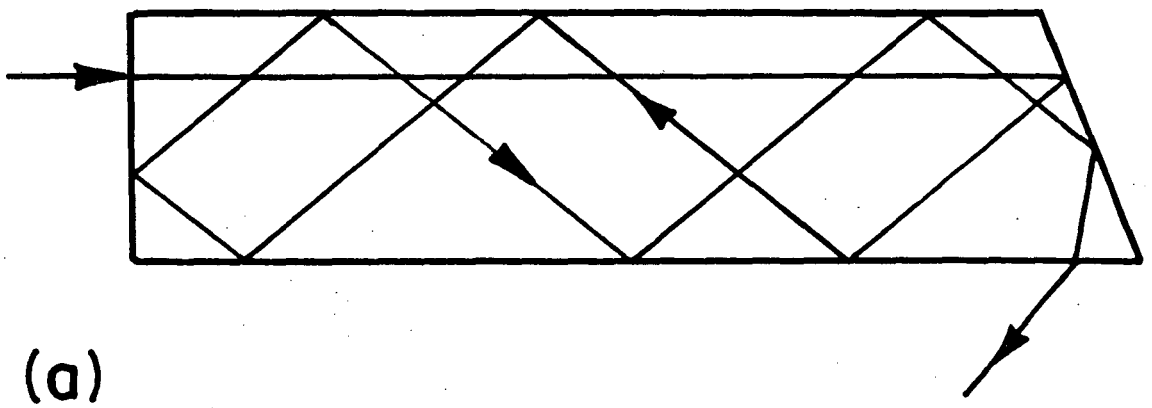

(a)

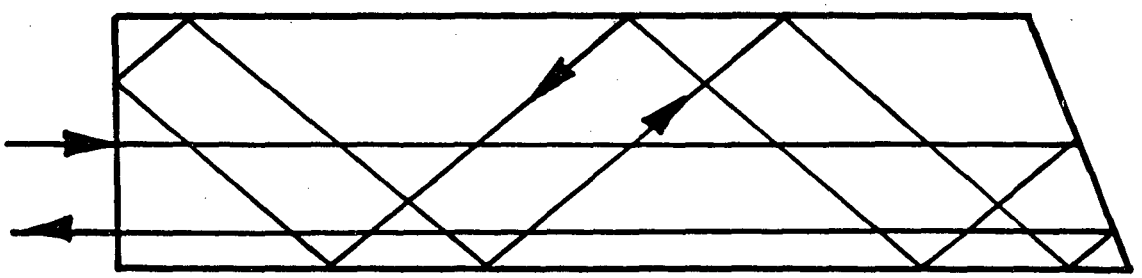

(b)

FIGURE 4

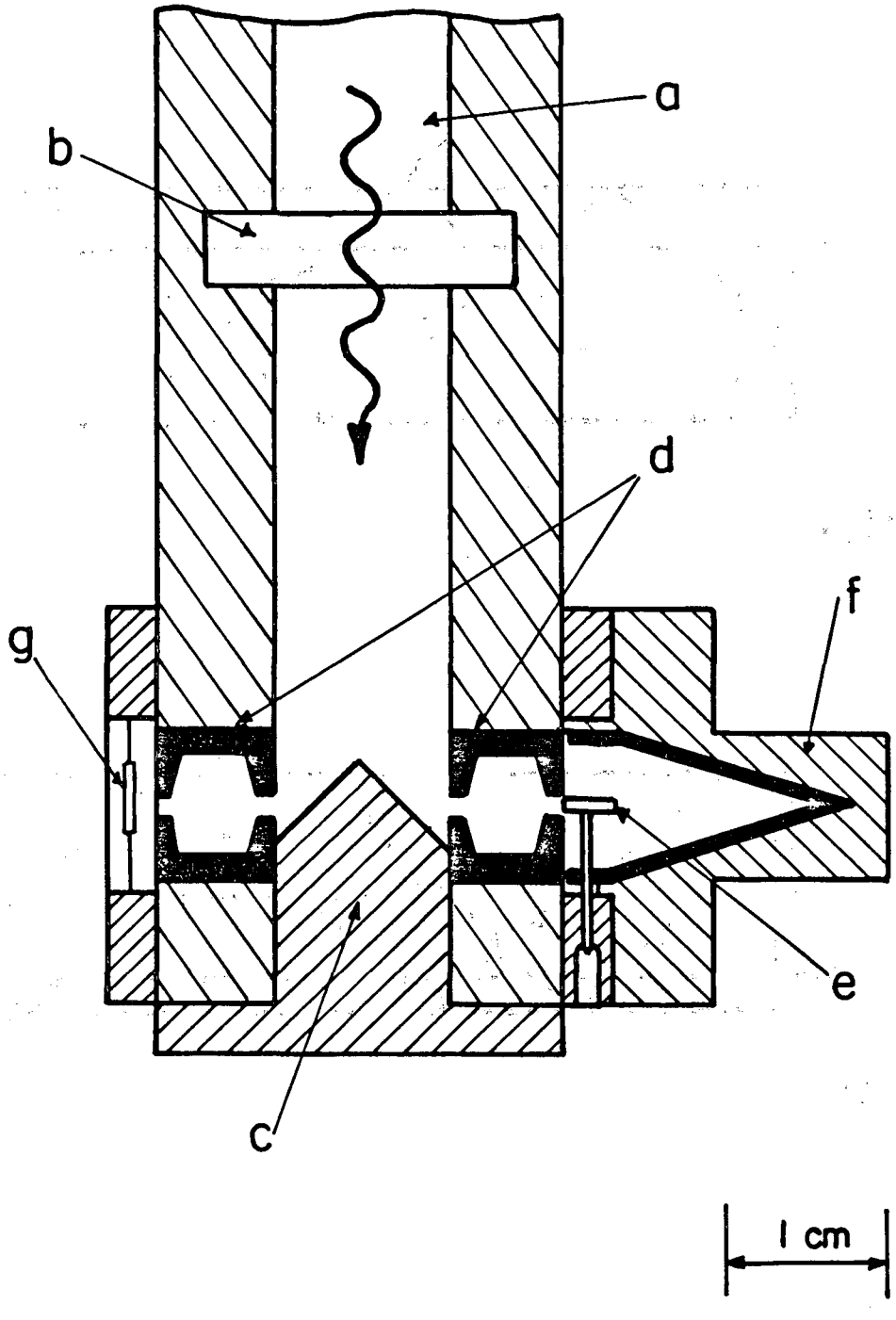

FIGURE 5

LAWRENCE BERKELEY LABORATORY
TECHNICAL INFORMATION DEPARTMENT
UNIVERSITY OF CALIFORNIA
BERKELEY, CALIFORNIA 94720